Civil Engineering Infrastructures Journal, 48(2): 235-250, December 2015
ISSN: 2322-2093

Dynamic Analysis of Cylindrically Layered Structures Reinforced by Carbon Nanotube Using MLPG Method

Ghouhestani, S.[1], Shahabian, F.[2*] and Hosseini, S.M.[3]

[1] PhD Candidate, Department of Civil Engineering, Faculty of Engineering, Ferdowsi University of Mashhad, Mashhad, Iran.

[2] Professor, Department of Civil Engineering, Faculty of Engineering, Ferdowsi University of Mashhad, Mashhad, Iran.

[3] Associate Professor, Department of Industrial Engineering, Faculty of Engineering, Ferdowsi University of Mashhad, Mashhad, Iran.

Received: 25 Feb. 2014 Revised: 17 Feb. 2015 Accepted: 10 Mar. 2015

Abstract: This paper deals with the dynamic analysis of stress field in cylindrically layered structures reinforced by carbon nanotube (CLSRCN) subjected to mechanical shock loading. Application of meshless local integral equations based on meshless local Petrov-Galerkin (MLPG) method is developed for dynamic stress analysis in this article. Analysis is carried out in frequency domain by applying the Laplace transformation on governing equations and then the stresses are transferred to time domain, using Talbot inversion Laplace techniques. The mechanical properties of the nanocomposite are mathematically simulated using four types of carbon nanotube distributions in radial volume fraction forms. The propagation of stresses is indicated through radial direction for various grading patterns at different time instants. The effects of various grading patterns on stresses are specifically investigated. Numerical examples, presented in the accompanying section 4 of this paper, show that variation of V_{CN}^{*} has no significant effect on the amplitude of radial stresses. Examples illustrate that stress distributions in cylindrical layer structures made of a CNT type Λ are more sensitive rather than other grading pattern types of CNTs. Results derived in this analysis are compared with FEM and previous published work and a good agreement is observed between them.

Keywords: Carbon nanotube, Cylinder, Dynamic analysis, Layered-structures, Meshless local Petrov-Galerkin method.

INTRODUCTION

Laminated fiber reinforced composites are widely used in light weight structures. Recently, a new member of the advanced material family called carbon nanotube-reinforced composites was introduced by Esawi et al. (2007). Carbon nanotubes with particular stiffness and strength have been noted as ideal reinforcements of composites. Carbon nanotubes, which are graphitic sheets rolled into seamless tubes, are a new nanoscale material discovered by Iijima (1991). These materials are currently receiving much attention due to their interesting properties, and various methods have been presented for assessing their attributes. Lu (1997) presented an experimental model for prediction of the elastic attributes of single and multilayered nanotubes.

The literature review revealed that the dynamic problem and wave propagation

∗ Corresponding author Email: shahabf@um.ac.ir

analysis of FGMs have been carried out. Gilhooley et al. (2008) employed the MLPG method for two-dimensional stress analysis of functionally graded solids, using radial basis functions. In their work, static and dynamic deformations of functionally graded materials (FGMs) were studied in detail, considering both linear elastic and linear viscoelastic simulations. The dispersion behavior of waves in a functionally graded elastic plate was studied using laminate plate theory by Chen et al. (2007). Hosseini et al. (2007) studied dynamic response and radial wave propagation velocity in thick hollow cylinder made of FGMs. They solved the Navier equation using the Galerkin finite element and Newmark methods. Scattering relations were obtained by considering the continuity conditions at the interfaces between any two layers and the boundary conditions at the upper and lower surfaces. In another work, elastic radial wave propagation and dynamic analysis of functionally graded thick hollow cylinders was studied by Hosseini and Abolbashari (2010). They proposed an analytical method for the dynamic response analysis of functionally graded thick hollow cylinders under impact loading. Bahmyari and Rahbar-ranji (2012) applied element free Galerkin method for free vibration analysis of orthotropic plates with variable thickness resting on non-uniform elastic foundation. They considered the effects of thickness variation, foundation parameter and boundary conditions on frequency. The thermo-elastic wave propagation was stochastically studied using a hybrid numerical method (GFE, NFD and Monte Carlo simulation) for isotropic and functionally graded thick hollow cylinder by Hosseini and Shahabian (2011a,b). Similar to this study, in the design and analysis of laminated composite cylinders, axisymmetric loads and axisymmetric geometries were often assumed for developing closed-form analytic solutions. In addition, the cylinder is assumed to have an infinite length such that the stresses are not only independent of the circumferential coordinate but also independent of the axial coordinate.

Approximate solutions of realistic engineering problems are usually obtained numerically. Recently, many meshless methods have been proposed to solve these problems (Sladek et al., 2013). Meshless methods such as the element-free Galerkin (EFG) method, the Reproducing Kernel particle method (RKPM), hp-clouds, the partition of unity method (PUM), the meshless local Petrov–Galerkin (MLPG) method, the smoothed particle hydrodynamics (SPH), the corrected smoothed particle hydrodynamics (CSPH), and the modified smoothed particle hydrodynamics (MSPH), have attracted considerable attention (Sladek et al., 2013).

Recently, radial basis functions (RBFs) have been employed to solve partial differential equations and to approximate the trial function in meshless methods (Singh et al., 2011). The modified multi quadrics (MQ) and the thin plate spline (TPS) radial basis functions have been successfully employed to approximate a trial solution in the MLPG formulation (Xiao et al., 2003) for solving 2D elastic problems. The MQ and TPS radial basis functions have been employed for the analysis of homogeneous and laminated plates (Xiao et al., 2008). Singh et al. (2013) used meshless collocations method by applying Gaussian and MQ radial basis functions, for the stability analysis of orthotropic and cross ply laminated composite plates subjected to thermal mechanical loading. Meshless methods have been used to analyze deformations of structures comprised of FGMs. Ching et al. (2005) used the MLPG method with test function equal to the weight function, to generate the MLS basis function for the study of transient thermoelastic deformations of FG solids.

In this study, the transient stress analysis of multilayered FG nanocomposite cylinder reinforced by carbon nanotube is investigated for four types of nanocomposites, using MLPG method. In MLPG method, a Heaviside step function was assumed to be a test function. The obtained results are compared with data reported in previous studies. The application of MLPG method has a high capability to study the effects of carbon nanotubes with grading distributions for reinforcement of composite structures.

Contributions of this work include using the performance of the MLPG method, for a class of dynamic problems for non-homogenous layered bodies. It is found that for dynamic problems, the MLPG method give results that compare very well with those obtained in previous research.

Programs of the MLPG method are developed in MATLAB, and a number of numerical examples of free vibration analysis are presented to demonstrate the present method. The effect of some important parameters such as CNT types and CNT volume fractions on the stress wave propagation at the different points of cylindrical layered structures reinforced by CNT is also investigated thoroughly, and the results are presented in details.

MATERIAL PROPERTIES OF CARBON NANOTUBE

Consider a cylindrically layered structure with three layers in which the inner and outer layers are made of functionally graded materials and middle layer is isotropic. In this paper, each carbon nanotube reinforced composite (CNTRC) layer is made from a mixture of SWCNT, graded distribution in the radial direction, and material matrix with isotropic material property. Various micromechanical models have been proposed to calculate the effective material properties of CNTRCs (Seidel et al., 2006).

According to the extended rule of mixture, the effective Young's modulus and shear modulus can be found as (Shen, 2009):

$$E_1 = \xi_1 V_{CN} E_1^{CN} + V_m E^m \tag{1}$$

$$\frac{\xi_2}{E_2} = \frac{V_{CN}}{E_2^{CN}} + \frac{V_m}{E_m} \tag{2}$$

$$\frac{\xi_3}{G_{12}} = \frac{V_{CN}}{G_{12}^{CN}} + \frac{V_m}{G_m} \tag{3}$$

$$\rho = V_{CN} \rho^{CN} + V_m \rho^m \tag{4}$$

$$\upsilon_{ij} = V_{CN} \upsilon_{ij}^{CN} + \mathrm{V}_m \upsilon^m \qquad i, j = 1, 2, 3 \quad i \neq j \tag{5}$$

$$V_{CN} + V_m = 1 \tag{6}$$

where $E_1^{CN}, \mathrm{E}_2^{CN}, G_{12}^{CN}, \upsilon^{CN}$ and ρ^{CN}: are elasticity modulus, shear modulus, Poisson's ratio and density of the carbon nanotube, respectively, and $E^m, G^m, \upsilon^m, \rho^m$: are corresponding properties for the matrix. The parameters V_{CN} and V_m: are volume fractions of carbon nanotube and matrix, respectively. The subscripts *CN* and *m*: stand for carbon nanotube and matrix. The terms $\xi_J\ (J = 1, 2, 3)$: are CNT efficiency parameters. Four types of variation of CNT along the radial direction of cylinder were proposed as follows (Figure 1).

$$V_{CN} = \begin{cases} V_{CN}^* & type\ UD \\ 2\left(\dfrac{r_0 - r}{r_0 - r_i}\right) V_{CN}^* & type\ V \\ 2\left(\dfrac{r - r_i}{r_0 - r_i}\right) V_{CN}^* & type\ \Lambda \\ 4\left|\dfrac{r - r_m}{r_0 - r_i}\right| V_{CN}^*, \quad r_m = \dfrac{r_i + r_0}{2} & type\ X \end{cases} \tag{7}$$

where

$$V_{CN}^* = \frac{\rho_m}{m_{CN} + \left(\dfrac{\rho_{CN}}{w_{CN}}\right) - \rho_{CN}} \tag{8}$$

The term m_{CN}: is the mass fraction of nanotube.

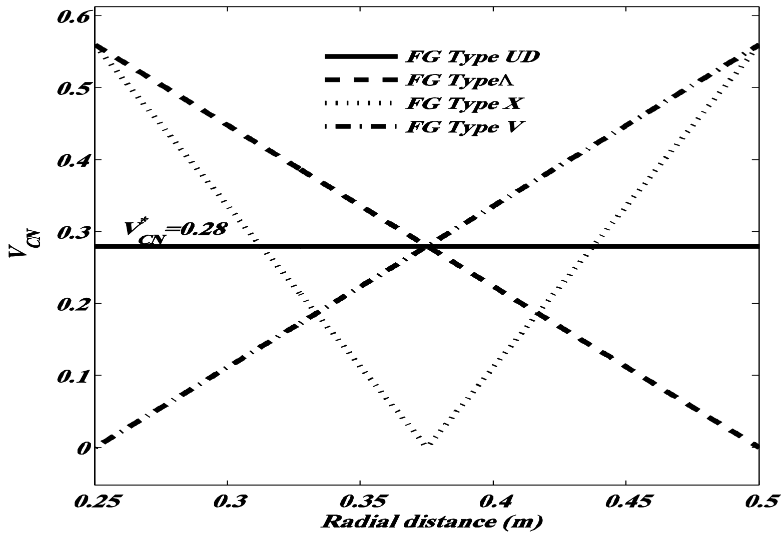

Fig. 1. Four types of variation of nanotube volume fraction (V_{CN}) along the radial direction

Basic Formulations

Considering a 2D elasto-dynamic problem, the constitutive equations in a domain Ω are written as:

$$\frac{\partial\sigma_{rr}}{\partial r}+\frac{\partial\tau_{rz}}{\partial z}+\frac{1}{r}(\sigma_{rr}-\sigma_{\theta\theta})+B_r = \rho(r,z)\frac{\partial^2 u_r}{\partial t^2} \tag{9}$$

$$\frac{\partial\tau_{rz}}{\partial r}+\frac{\partial\sigma_{zz}}{\partial z}+\frac{1}{r}\tau_{rz}+B_z = \rho(r,z)\frac{\partial^2 u_z}{\partial t^2} \tag{10}$$

According to Hook's law:

$$\sigma=[D]\varepsilon \tag{11}$$

where

$$\sigma^T=\{\sigma_{rr}\ \ \sigma_{\theta\theta}\ \ \sigma_{zz}\ \ \tau_{rz}\} \tag{12}$$

$$\begin{aligned}&\varepsilon^T=\{\varepsilon_{rr}\ \ \varepsilon_{\theta\theta}\ \ \varepsilon_{zz}\ \ \varepsilon_{rz}\}\\&\varepsilon_{rr}=\frac{\partial u_r}{\partial r}\quad \varepsilon_{\theta\theta}=\frac{u_r}{r}\\&\varepsilon_{zz}=\frac{\partial u_z}{\partial z}\quad \varepsilon_{rz}=\frac{\partial u_z}{\partial r}+\frac{\partial u_r}{\partial z}\end{aligned} \tag{13}$$

where σ and ε: are the stress and strain tensors, u_r, u_z and B_r, B_z: are the displacement and body force components, respectively, and ρ: is the mass density. D: denotes for the elastic constants, which are defined as follows:

$$\begin{bmatrix}D_{11}(r) & D_{12}(r) & D_{13}(r) & 0\\ D_{21}(r) & D_{22}(r) & D_{23}(r) & 0\\ D_{31}(r) & D_{32}(r) & D_{33}(r) & 0\\ 0 & 0 & 0 & D_{55}(r)\end{bmatrix} \tag{14}$$

where

$$\begin{aligned}&D_{11}(r)=\frac{1-\upsilon_{23}(r)\upsilon_{32}(r)}{E_2(r)E_3(r)\lambda},\ D_{22}(r)=\frac{1-\upsilon_{31}(r)\upsilon_{13}(r)}{E_1(r)E_3(r)\lambda},\ D_{33}=\frac{1-\upsilon_{21}(r)\upsilon_{12}(r)}{E_1(r)E_2(r)\lambda}\\&D_{12}(r)=\frac{\upsilon_{21}(r)+\upsilon_{31}(r)\upsilon_{23}(r)}{E_2(r)E_3(r)\lambda},\ D_{23}(r)=\frac{\upsilon_{32}(r)+\upsilon_{12}(r)\upsilon_{31}(r)}{E_1(r)E_3(r)\lambda}\\&D_{13}(r)=\frac{\upsilon_{31}(r)+\upsilon_{21}(r)\upsilon_{32}(r)}{E_2(r)E_3(r)\lambda},\ D_{55}(r)=G_{12}(r)\end{aligned} \tag{15}$$

$$\lambda=\frac{1-\upsilon_{32}(r)\upsilon_{23}(r)-\upsilon_{21}(r)\upsilon_{12}(r)-\upsilon_{13}(r)\upsilon_{31}(r)-2\upsilon_{32}(r)\upsilon_{21}(r)\upsilon_{13}(r)}{E_1(r)E_2(r)E_3(r)} \tag{16}$$

In this study, it was assumed that the body force is zero.

Local Weak Form

A weak form of Eqs. (9) and (10) in polar coordinate over a subdomain Ω_q which is bounded by Γ_q as shown in Figure 2, obtained using the weighted residual method is:

$$\int_{\Omega_q} \left\{ \begin{array}{l} \dfrac{\partial \sigma_{rr}}{\partial r} + \dfrac{\partial \tau_{rz}}{\partial z} \\ + \dfrac{1}{r}\left(\sigma_{rr} - \sigma_{\theta\theta}\right) \\ -\rho(r,z)\dfrac{\partial^2 u_r}{\partial t^2} \end{array} \right\} r W_r(r,z)\, d\Omega = 0 \qquad (17)$$

$$\int_{\Omega_q} \left\{ \begin{array}{l} \dfrac{\partial \tau_{rz}}{\partial r} + \dfrac{\partial \sigma_{zz}}{\partial z} \\ + \dfrac{1}{r}\tau_{rz} \\ -\rho(r,z)\dfrac{\partial^2 u_z}{\partial t^2} \end{array} \right\} r W_z(r,z)\, d\Omega = 0 \qquad (18)$$

where $W_r(r,z)$ and $W_z(r,z)$ are the weighted functions at the field node I .

By applying divergence theorem relation in the above equations, it can be concluded that:

$$\int_{\Omega_q} \left(\begin{array}{l} r\,\tau_{rz}\,\dfrac{\partial W_z(r,z)}{\partial r} \\ + r\,\sigma_{zz}\,\dfrac{\partial W_z(r,z)}{\partial z} \end{array} \right) d\Omega - \int_{\Gamma_q} r W_z(r,z)\left(n_r \tau_{rz} + n_z \sigma_{zz}\right) d\Gamma + \int_{\Omega_q} \rho(r,z)\frac{\partial^2 u_z(r,z,t)}{\partial t^2} W_z(r,z)\, r\, d\Omega = 0 \qquad (19)$$

$$\int_{\Omega_q} \left(\begin{array}{l} r\,\dfrac{\partial W_r(r,z)}{\partial r}\sigma_{rr} \\ + W_r(r,z)\sigma_{\theta\theta} \\ + r\,\dfrac{\partial W_r(r,z)}{\partial z}\tau_{rz} \end{array} \right) d\Omega - \int_{\Gamma_q} r W_r(r,z)\left(n_r \sigma_{rr} + n_z \tau_{rz}\right) d\Gamma + \int_{\Omega_q} \rho(r,z)\frac{\partial^2 u_r(r,z,t)}{\partial t^2} W_r(r,z)\, r\, d\Omega = 0 \qquad (20)$$

The test and trial function can be chosen from different functional spaces. Here, having chosen the test function as the Heaviside unit step function with support on the local subdomain.

$$\mathrm{W}_r(r,z) = \mathrm{W}_z(r,z) = \begin{cases} 1 \ , & r,z \in \Omega_q \\ 0 \ , & r,z \notin \left(\Omega_q \cup \Gamma_q\right) \end{cases} \qquad (21)$$

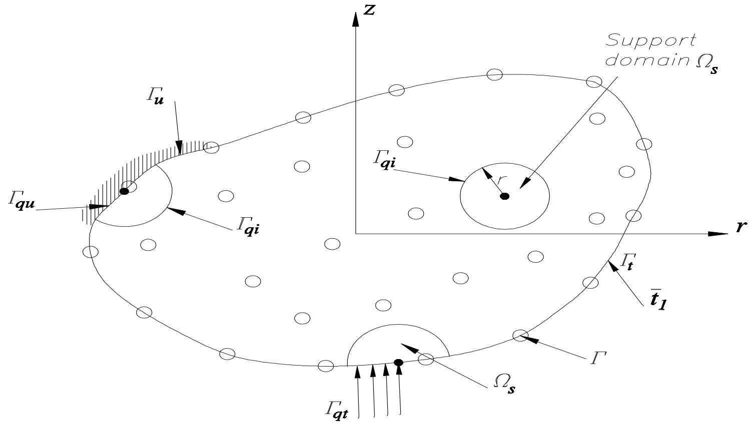

Fig. 2. Local domains used in the MLPG method

where Γ_q : is composed of three parts, i.e., $\Gamma_q = \Gamma_{qi} \cup \Gamma_{qu} \cup \Gamma_{qt}$ as shown in Figure 2. Here Γ_{qi} : is the internal boundary of the quadrature domain, which does not intersect the global boundary Γ; Γ_{qu} : is the part of the prescribed generalized displacement boundary that intersects the quadrature domain, i.e., $\Gamma_{qu} = \Gamma_q \cap \Gamma_u$; Γ_{qt} : is the part of the prescribed generalized traction boundary that intersects the quadrature domain, i.e., $\Gamma_{qt} = \Gamma_q \cap \Gamma_t$.

$$\int_{\Omega_q} \begin{pmatrix} r\dfrac{\partial W_r(r,z)}{\partial r}\sigma_{rr} \\ +W_r(r,z)\sigma_{\theta\theta} \\ +r\dfrac{\partial W_r(r,z)}{\partial z}\tau_{rz} \end{pmatrix} d\Omega - \int_{\Gamma_{qi}+\Gamma_{qu}} rW_r(r,z)(n_r\sigma_{rr} + n_z\tau_{rz})d\Gamma + \int_{\Omega_q} \rho(r,z)\frac{\partial^2 u_r(r,z,t)}{\partial t^2} W_r(r,z)\, r\, d\Omega = \int_{\Gamma_{qt}} rW_r(r,z)(n_r\sigma_{rr} + n_z\tau_{rz})d\Gamma \tag{22}$$

$$\int_{\Omega_q} \begin{pmatrix} r\,\tau_{rz}\dfrac{\partial W_z(r,z)}{\partial r} \\ +r\,\sigma_{zz}\dfrac{\partial W_z(r,z)}{\partial z} \end{pmatrix} d\Omega - \int_{\Gamma_{qi}+\Gamma_{qu}} rW_z(r,z)(n_r\tau_{rz} + n_z\sigma_{zz})d\Gamma + \int_{\Omega_q} \rho(r,z)\frac{\partial^2 u_z(r,z,t)}{\partial t^2} W_z(r,z)\, r\, d\Omega = \int_{\Gamma_{qt}} rW_z(r,z)(n_r\tau_{rz} + n_z\sigma_{zz})d\Gamma \tag{23}$$

in which

$$t_r = n_r\sigma_{rr} + n_z\tau_{rz} \tag{24}$$

$$t_z = n_z\sigma_{zz} + n_r\tau_{rz} \tag{25}$$

where t_r and t_z : are radial and axial tractions respectively, and n_r and n_z : are unit vectors in r and z directions, respectively.

Interpolation Using Radial Basis Functions

In the MLPG method, the global domain of the problem was divided into many subdomains, a weak-form over the local sub-domains such as "Ω_q" was constructed. These sub-domains can overlap with each other, and cover the whole global domain (Figure 2). The local sub-domains could be of any geometric shape such as circle and rectangular with various sizes. In the present paper, the local sub-domains were taken to be of a circular shape for simplicity. In such a case, the calculation of domain-integrals is quite easy.

In this study, the Laplace transformation was used to solve the time domain equilibrium equation. According to Eqs. (22) and (23), by using Laplace Transformation concept the proposed relationship is as follows.

$$\int_{\Omega_q} \left\{ \begin{matrix} r\dfrac{\partial W_r(r,z)}{\partial r}\mathrm{L}(\sigma_{rr}(r,z,s)) \\ +W_r(r,z)\mathrm{L}(\sigma_{\theta\theta}(r,z,s)) \\ +r\dfrac{\partial W_r(r,z)}{\partial z}L(\tau_{rz}(r,z,s)) \end{matrix} \right\} d\Omega - \int_{\Gamma_{qi}+\Gamma_{qu}} rW_r(r,z)\begin{bmatrix} n_r\mathrm{L}(\sigma_{rr}(r,z,s)) \\ +n_z L(\tau_{rz}(r,z,s)) \end{bmatrix} d\Gamma + \int_{\Omega_q} rW_r(r,z)\rho(r,z) \begin{bmatrix} s^2 L(u_r(r,z,s)) - su_r \\ (r,z,0) - \dot{u}_r(r,z,0) \end{bmatrix} d\Omega = \int_{\Gamma_{qt}} rW_r(r,z)L(t_r)d\Gamma \tag{26}$$

$$\int_{\Omega_q}\left\{\begin{array}{l} r\dfrac{\partial W_z(r,z)}{\partial r}L(\tau_{rz}(r,z,s)) \\ +r\dfrac{\partial W_z(r,z)}{\partial z}\mathrm{L}(\sigma_{zz}(r,z,s)) \end{array}\right\}d\Omega$$
$$-\int_{\Gamma_{qi}+\Gamma_{qu}} rW_z(r,z)\begin{bmatrix} n_r L(\tau_{rz}(r,z,s)) \\ +n_z \mathrm{L}(\sigma_{zz}(r,z,s)) \end{bmatrix}d\Gamma$$
$$rW_z(r,z)\rho(r,z)$$
$$+\int_{\Omega_q}\begin{bmatrix} s^2L(u_z(r,z,s)) \\ -su_z(r,z,0)-\dot{u}_z(r,z,0) \end{bmatrix}d\Omega$$
$$=\int_{\Gamma_{qt}} rW_z(r,z)L(t_z)d\Gamma \tag{27}$$

he multilayer cylindrical structure is discretized by the nodes located on the problem domain. The nodal variable is a fictitious displacement component (r, z), in the polar coordinate system. In the MLPG method, the trial function was chosen to be the interpolation over a number of nodes randomly distributed within the domain of influence. For the spatial distribution of function "u", we applied the meshless approximation over a number of nodes randomly distributed within the domain of influence, using the radial basis function (RBF). Thus, components displacement variable can be expressed as:

$$u_r(r,z,t)=u_r(\bar{r},t)=\sum_{i=1}^{n}R_i(\bar{r})a_{r_i} = R^T(\bar{r})a_r(t) \qquad \forall r,z\in\Omega_q \tag{28}$$

$$u_z(r,z,t)=u_z(\bar{r},t)=\sum_{i=1}^{n}R_i(\bar{r})a_{z_i} = R^T(\bar{r})a_z(t) \qquad \forall r,z\in\Omega_q \tag{29}$$

$$\bar{r}=\left[(r-r_i)^2+(z-z_i)^2\right]^{0.5} \tag{30}$$

where a_{r_i} and a_{z_i} are the coefficients for the radial basis $R_i(\bar{r})$ that is:

$$R_i(\bar{r})=\left[\bar{r}^2+\bar{c}^2\right]^q \tag{31}$$

where the terms $\bar{c}$ and q are constant positive values. The number of radial basis functions n was determined by the number of nodes in the support domain. This form of shape function has been widely used in surface fitting and in constructing approximate solutions for partial differential equations. The vector R has the form:

$$R^T(\bar{r})=\left[R_1(\bar{r}),R_2(\bar{r}),....,R_n(\bar{r})\right] \tag{32}$$

which are the set of radial basis functions centered around "r_i", and vectors a_r and a_z : are defined as:

$$a_r^T(t)=\left\{a_{r_1},a_{r_2},a_{r_3},....,a_{r_n}\right\}, \quad a_z^T(t)=\left\{a_{z_1},a_{z_2},a_{z_3},....,a_{z_n}\right\} \tag{33}$$

From the interpolation Eqs. (28) and (29) for the radial functions, the following system of linear equation for the coefficients "a_r" and "a_z" were obtained as:

$$R_0a_r(t)=\tilde{u}_r(t),\; R_0a_z(t)=\tilde{u}_z(t) \tag{34}$$

where

$$\tilde{u}_r^T(t)=\left[u_r^1(t),u_r^2(t),\ldots,u_r^n(t)\right], \quad \tilde{u}_z^T(t)=\left[u_z^1(t),u_z^2(t),\ldots,u_z^n(t)\right] \tag{35}$$

are respectively composed of the time variable nodal values of displacements "$\tilde{u}_r^i(t)$" and "$\tilde{u}_z^i(t)$" while R_0 : is the matrix defined by nodal values of the RBFs as:

$$\begin{bmatrix} R_1(\bar{r}_1) & R_2(\bar{r}_1) & \cdots & R_n(\bar{r}_1) \\ R_1(\bar{r}_2) & R_2(\bar{r}_2) & \cdots & R_n(\bar{r}_2) \\ R_1(\bar{r}_n) & R_2(\bar{r}_n) & \cdots & R_n(\bar{r}_n) \end{bmatrix} \tag{36}$$

To calculate the vector "$a_r(t)$" and "$a_z(t)$", we can write from Eq. (34).

$$a_r(t)=R_0^{-1}\tilde{u}_r(t)\ ,\ a_z(t)=R_0^{-1}\tilde{u}_z(t) \tag{37}$$

The approximated function can be expressed in terms of the nodal values and the shape function as:

$$u_r(r,z,t)=R^T(\bar{r})R_0^{-1}\tilde{u}_r(t)=\Phi^T(\bar{r})\tilde{u}_r(t)=\sum_{a=1}^{n}\phi^a(\bar{r})u_r^a(t) \tag{38}$$

$$u_z(r,z,t)=R^T(\bar{r})R_0^{-1}\tilde{u}_z(t)=\Phi^T(\bar{r})\tilde{u}_z(t)=\sum_{a=1}^{n}\phi^a(\bar{r})u_z^a(t) \tag{39}$$

where $\phi^i(\bar{r})$: is the shape function associated with the node *i*. The nodal shape functions are given by:

$$\phi^T(\bar{r})=R^T(\bar{r})R_0^{-1} \tag{40}$$

By extending the Eq. (11), it can be concluded that:

$$\begin{aligned}
&\sigma_{rr}=D_{11}(r)\varepsilon_{rr}+D_{12}(r)\varepsilon_{\theta\theta}\\
&+D_{13}(r)\varepsilon_{zz}\ ,\ \sigma_{\theta\theta}=D_{21}(r)\varepsilon_{rr}\\
&+D_{22}(r)\varepsilon_{\theta\theta}+D_{23}(r)\varepsilon_{zz}\\
&\sigma_{zz}=D_{31}(r)\varepsilon_{rr}+D_{32}(r)\varepsilon_{\theta\theta}\\
&+D_{33}(r)\varepsilon_{zz}\ ,\ \tau_{rz}=D_{55}(r)\varepsilon_{rz}
\end{aligned} \tag{41}$$

By substituting Eqs. (38) and (41) in Eq. (26):

$$\begin{aligned}
&\int_{\Omega_q}\Bigg\{r\frac{\partial W_r(r,z)}{\partial r}\Bigg[D_{11}(r)\sum_{a=1}^{n}\frac{\partial\phi^a(\bar{r})}{\partial r}L(u_r^a(s))+\frac{D_{12}(r)}{r}\sum_{a=1}^{n}\phi^a(\bar{r})L(u_r^a(s))+D_{13}(r)\sum_{a=1}^{n}\frac{\partial\phi^a(\bar{r})}{\partial z}L(u_z^a(s))\Bigg]\\
&+W_r(r,z)\Bigg[D_{21}(r)\sum_{a=1}^{n}\frac{\partial\phi^a(\bar{r})}{\partial r}L(u_r^a(s))+\frac{D_{22}(r)}{r}\sum_{a=1}^{n}\phi^a(\bar{r})L(u_r^a(s))+D_{23}(r)\sum_{a=1}^{n}\frac{\partial\phi^a(\bar{r})}{\partial z}L(u_z^a(s))\Bigg]\\
&+r\frac{\partial W_r(r,z)}{\partial z}D_{55}(r)\Bigg[\sum_{a=1}^{n}\frac{\partial\phi^a(\bar{r})}{\partial r}L(u_z^a(s))+\sum_{a=1}^{n}\frac{\partial\phi^a(\bar{r})}{\partial z}\mathrm{L}(\mathrm{u}_r^a(s))\Bigg]\Bigg\}d\Omega\\
&-\int_{\Gamma_{q_i}+\Gamma_{q_u}}rW_r(r,z)\Bigg\{n_r\Bigg[D_{11}(r)\sum_{a=1}^{n}\frac{\partial\phi^a(\bar{r})}{\partial r}L(u_r^a(s))+\frac{D_{12}(r)}{r}\sum_{a=1}^{n}\phi^a(\bar{r})L(u_r^a(s))+D_{13}(r)\sum_{a=1}^{n}\frac{\partial\phi^a(\bar{r})}{\partial z}L(u_z^a(s))\Bigg]\\
&+n_zD_{55}(r)\Bigg[\sum_{a=1}^{n}\frac{\partial\phi^a(\bar{r})}{\partial r}L(u_z^a(s))+\sum_{a=1}^{n}\frac{\partial\phi^a(\bar{r})}{\partial z}\mathrm{L}(\mathrm{u}_r^a(s))\Bigg]\Bigg\}d\Gamma+\int_{\Omega_q}rW_r(r,z)\rho(r,z)\Bigg[s^2\sum_{a=1}^{n}\phi^a(r)L(u_r^a(s))\Bigg]d\Omega\\
&=\int_{\Gamma_{q_t}}rW_r(r,z)L(t_r)d\Gamma+\int_{\Omega_q}rW_r(r,z)\rho(r,z)\left[s\,u_r(r,z,0)+\dot{u}_r(r,z,0)\right]d\Gamma
\end{aligned} \tag{42}$$

Similar to the above equation, by substituting Eqs. (39) and (41) in Eq. (27):

$$\int_{\Omega_q}\left\{r\frac{\partial W_z(r,z)}{\partial r}D_{55}(r)\left[\sum_{a=1}^{n}\frac{\partial\phi^a(\bar{r})}{\partial r}L(u_z^a(s))+\sum_{a=1}^{n}\frac{\partial\phi^a(\bar{r})}{\partial z}\mathrm{L}(\mathrm{u}_r^a(s))\right]+r\frac{\partial W_z(r,z)}{\partial z}(r,z)\right.$$
$$\left.\times\left[D_{31}(r)\sum_{a=1}^{n}\frac{\partial\phi^a(\bar{r})}{\partial r}L(u_r^a(\mathrm{s}))+\frac{D_{32}(r)}{r}\sum_{a=1}^{n}\phi^a(\bar{r})L(u_r^a(\mathrm{s}))+D_{33}(r)\sum_{a=1}^{n}\frac{\partial\phi^a(\bar{r})}{\partial z}L(u_z^a(\mathrm{s}))\right]\right\}d\Omega$$
$$-\int_{\Gamma_{q_i}+\Gamma_{qu}}rW_z(r,z)\left\{n_rD_{55}(r)\left[\sum_{a=1}^{n}\frac{\partial\phi^a(\bar{r})}{\partial r}L(u_z^a(s))+\sum_{a=1}^{n}\frac{\partial\phi^a(\bar{r})}{\partial z}\mathrm{L}(\mathrm{u}_r^a(s))\right]\right.$$
$$\left.+n_z\left[D_{31}(r)\sum_{a=1}^{n}\frac{\partial\phi^a(\bar{r})}{\partial r}L(u_r^a(\mathrm{s}))+\frac{D_{32}(r)}{r}\sum_{a=1}^{n}\phi^a(\bar{r})L(u_r^a(\mathrm{s}))+D_{33}(r)\sum_{a=1}^{n}\frac{\partial\phi^a(\bar{r})}{\partial z}L(u_z^a(\mathrm{s}))\right]\right\}d\Gamma$$
$$+\int_{\Omega_q}rW_z(r,z)\rho(r,z)\left[s^2\sum_{a=1}^{n}\phi^a(\bar{r})L(u_z^a(s))\right]d\Omega$$
$$=\int_{\Gamma_{q_t}}rW_z(r,z)L(t_z)d\Gamma+\int_{\Omega_q}rW_z(r,z)\rho(r,z)\left[s\,u_z(r,z,0)+\dot{\mathrm{u}}_z(r,z,0)\right]d\Gamma \tag{43}$$

By inverse Laplace transform approaches such as Week's method, Post's formula or Talbot's method time-dependent values in previous equation can be calculated. In the present analysis, the time-dependent values of the transformed quantities in the previous consideration obtained by the Talbot method (Abate et al., 2004). The Talbot method is based on deformation of the Bromwich inversion integral contour. A good review of the above method is given in Davies (2002) study. In fact, we recommend reading that chapter because it provides a sense of numerical calculation considerations in a computing environment.

The formula for this method to numerically calculate $u_i(t)$ can be written as:

$$u_i(t)=\frac{2}{5t}\sum_{k=0}^{n-1}\Re e\left(\gamma_k u_i(S_k)\right),\ S_k=\frac{\delta_k}{t} \tag{44}$$

where n: is the number of samples and

$$\delta_0=\frac{2n}{5},\ \delta_k=\frac{2k\pi}{5}\left[\cot\left(\frac{k\pi}{n}\right)+i\right],\ i=\sqrt{-1}\quad 0<k<n \tag{45}$$

$$\gamma_0=\frac{1}{2}e^{\delta_0},\ \gamma_k=\left[\begin{array}{l}1+i\left(\frac{k\pi}{n}\right)\left(1+\left(\cot\left(\frac{k\pi}{n}\right)\right)^2\right)\\ -i\cot\left(\frac{k\pi}{n}\right)\end{array}\right]e^{\delta_0}\quad 0<k<n \tag{46}$$

NUMERICAL RESULTS AND DISCUSSION

In this study, to verify the presented method and results, a problem was solved with geometry and boundary conditions used by Moussavinezhad et al. (2013). The comparison between results obtained from the presented method with those reported by Moussavinezhad et al. (2013) show good agreement (Figure 3).

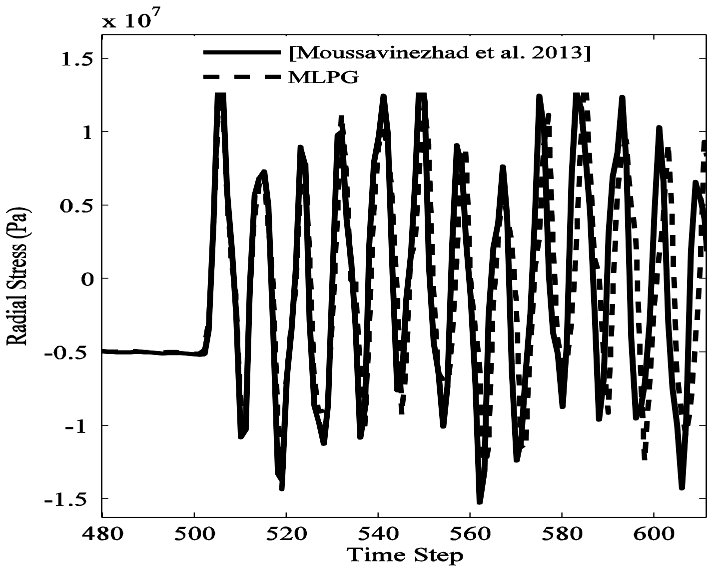

Fig. 3. The comparison of obtained results from MLPG with those using Moussavinezhad et al. (2013) for radial stress

The following boundary conditions and parameter values were used to verify the results.

$$\sigma_r(r_i, t) = P_i(t) \tag{47}$$

$$\sigma_r(r_o, t) = 0 \tag{48}$$

So that,

$$P_i(t) = \begin{cases} P_0 t & t \le t_0 \\ 0 & t > t_0 \end{cases} \tag{49}$$

where "$P_0 = 4GPa/Sec$" and "$t_0 = 0.005Sec$".

$$V_{CN} = V_m = 0 \tag{50}$$

$$\xi_1 = \xi_2 = \xi_3 = 1 \tag{51}$$

To show the accuracy and capability of the MLPG method, a multilayered composite cylinder with infinite length is presented with '$r_i = 0.25m$' and '$r_o = 0.5m$', which are inner radius and outer radius, respectively (Figure 4).

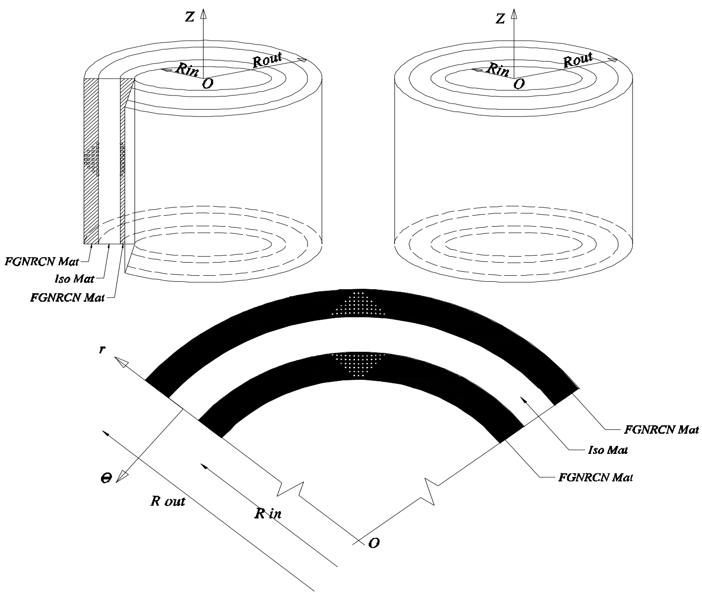

Fig. 4. Cylindrically layered structure with three layers

Table 1 shows the geometry properties of multilayered cylinder in which the inner and outer layers are made of FGCNTs with four types of distributions as shown in Figure 1. The middle layer is made of isotropic material. The inner and outer layers consist of polymethyl-methacrylate (PMMA) as matrix, with CNT as fibers aligned in the circumferential direction. Properties of these two kinds of materials are presented as:

For PMMA (Shen, 2011):

$E^m = 2.5GPa$, $\rho^m = 1150\,kg/m^3$, $\upsilon^m = 0.34$.

For SWCNT (Shen, 2011):

$E_1^{CN} = 5.6466TPa, E_2^{CN} = 7.0800TPa, G_{12}^{CN} = 1.9445TPa, \rho^{CN} = 1400\,kg/m^3, \upsilon_{12}^{CN} = 0.175.$

For middle layer:

$E_m = 70GPa, \rho_m = 2707\,kg/m^3, \upsilon_m = 0.3$.

The time histories of hoop and radial stresses of middle point on thickness of cylindrically layered structure are illustrated in Figure 5, for various types of V_{CN} distributions along the radial direction with $V_{CN}^* = 0.12$ and $V_{CN}^* = 0.28$.

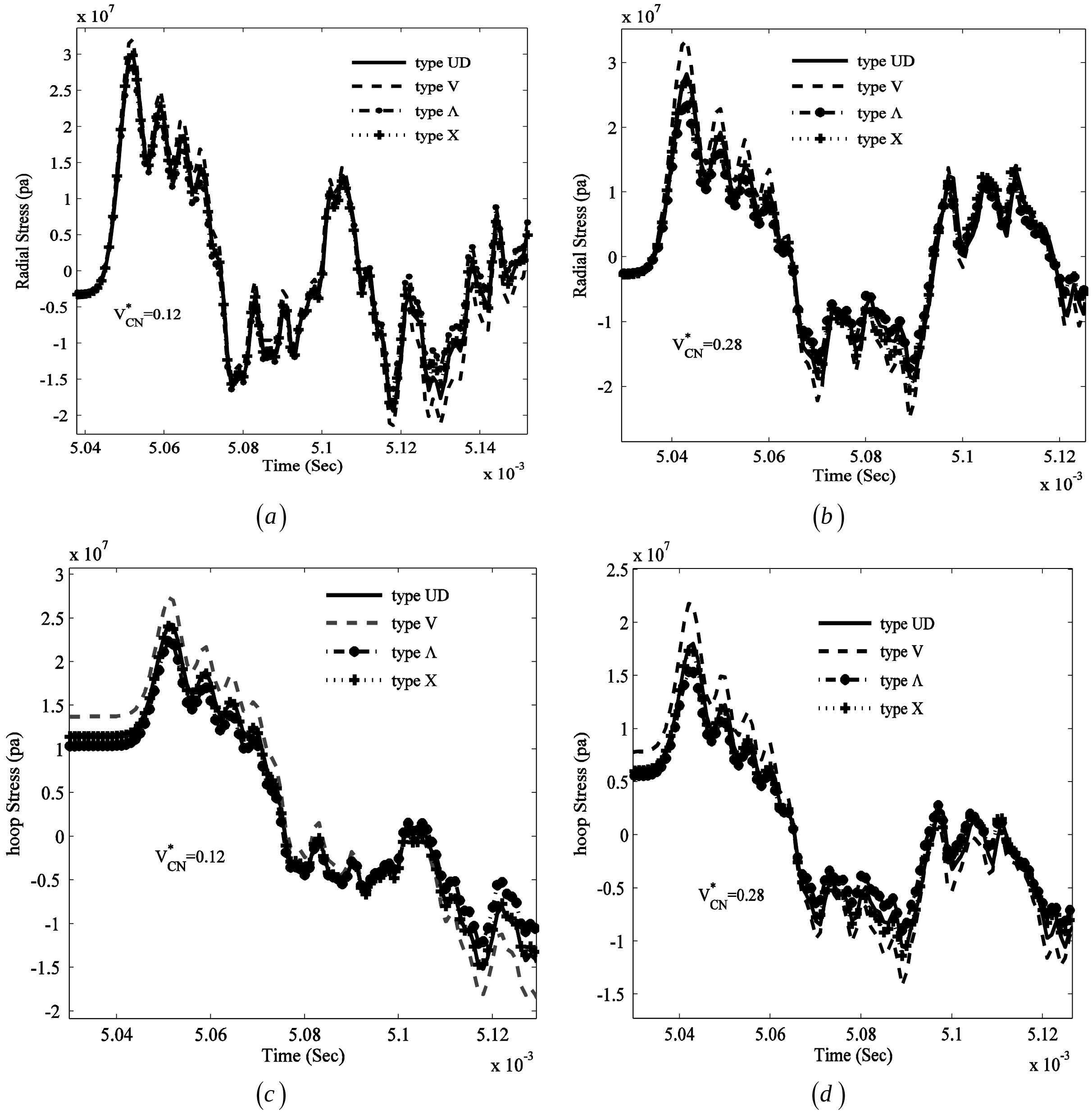

Fig. 5. Time history of radial stress and hoop stress for the middle point of cylinder thickness for various grading patterns of V_{CN}

Table 1. Geometry property of three layered cylinder

Position of layer	Thickness (cm)	r_{min} (cm)	r_{max} (cm)	Material type
inner layer	5	25	30	FGCNTs type1-4
middle layer	15	30	45	Iso
outer layer	5	45	50	FGCNTs type1-4

As shown in this figure, it can be concluded that CNT distribution types have little effect on the amplitude of radial stress as compared to hoop stress. By comparing stresses plotted in Figure 5, the following results can be obtained: First, the variation in CNTs type distributions along radial direction has more effect on the time history of hoop stress. Second, the maximum hoop stress and the maximum radial stress are achieved when CNT variation type is V . Third, the minimum hoop stress and minimum radial stress were achieved when CNT variation type is Λ .

Figures 6 and 7 depict the time history of radial stress and hoop stress at middle point on the thickness of multilayer nanocomposite cylinder for various values of V_{CN}^{*} and four types of CNTs distributions.

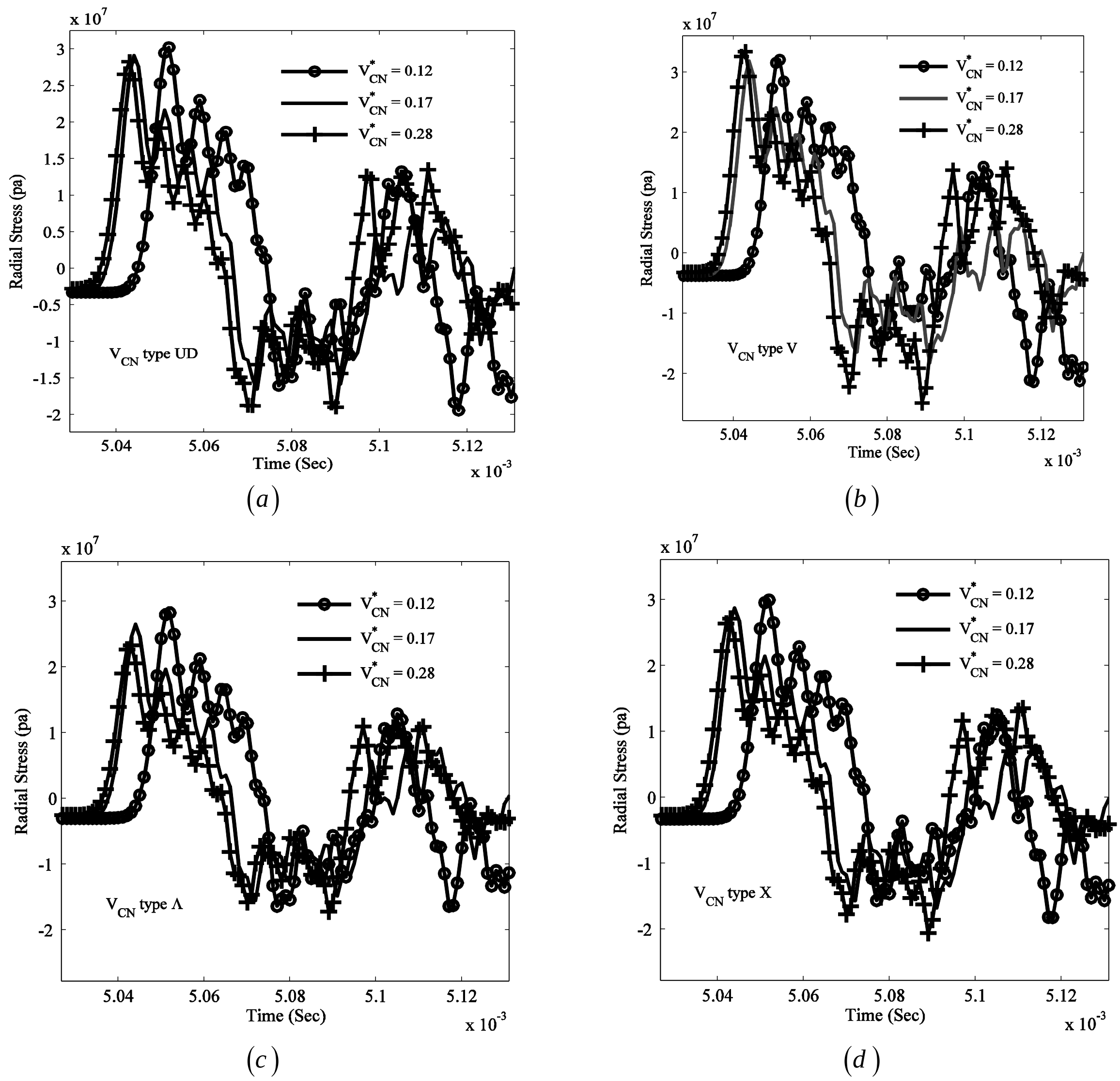

Fig. 6. Time history of radial stress at middle point of cylinder thickness for various values of V_{CN}^{*}

By comparing stresses plotted in these figures, it is concluded that the variation in V_{CN}^* reduces the magnitudes of hoop stress and has little effect on radial stress. These conclusions are further supported by results plotted in Figures (6c) and (7c), where stresses are plotted for Λ grading pattern with varying V_{CN}^*. These results imply that increasing V_{CN}^* leads to decreased hoop stresses as would be expected since the CNT is aligned in circumferential direction.

From these figures, it is understood that Λ grading pattern has more effect on reduction of hoop stress and V grading pattern has little effect on reduction of hoop stress with various values of V_{CN}^*. As an example, the layered cylinder with inner and outer layer made of Λ CNT grading pattern and isotropic middle layer with varying V_{CN}^* is analyzed here. Comparison of the radial stress and hoop stress at different point of layered cylinder is shown in Figure 8.

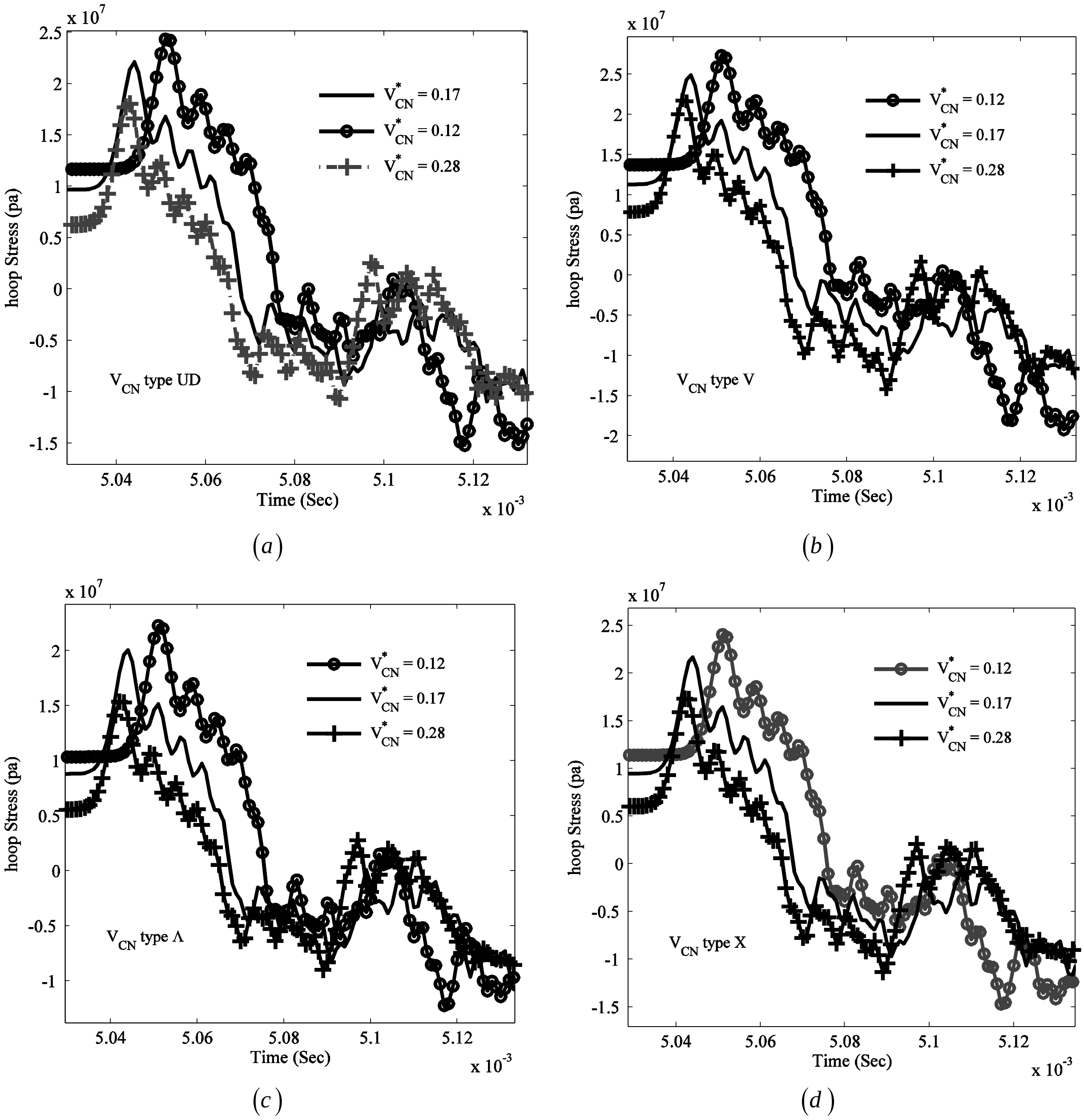

Fig. 7. Time history of hoop stress at middle point of cylinder thickness for various values of V_{CN}^*

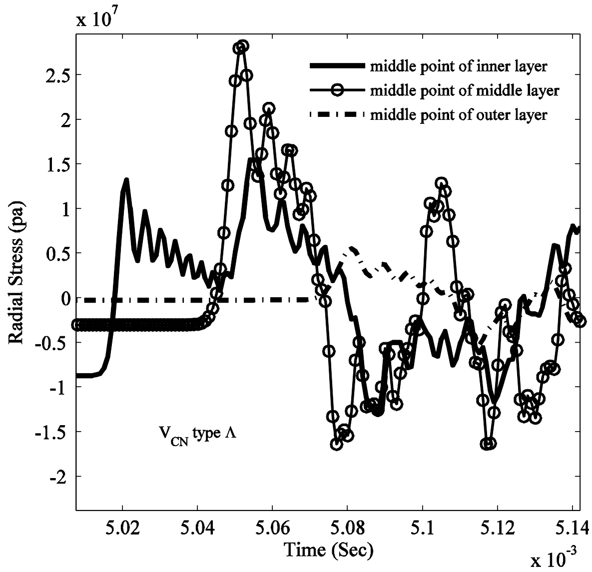

$(a): V_{CN}^{*} = 0.12$

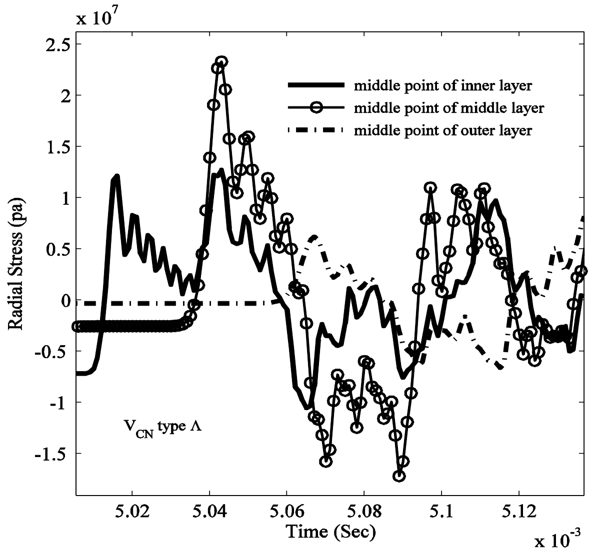

$(b): V_{CN}^{*} = 0.28$

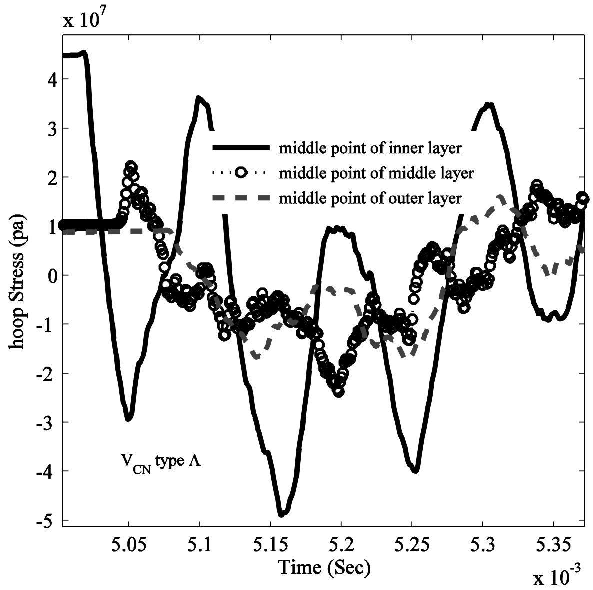

$(c): V_{CN}^{*} = 0.12$

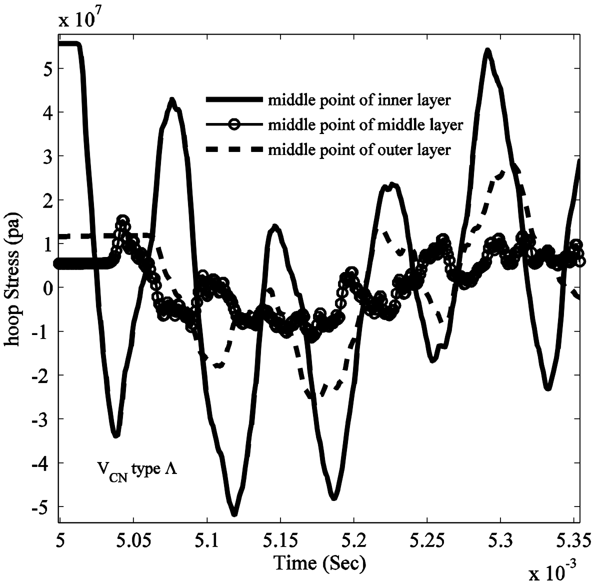

$(d): V_{CN}^{*} = 0.28$

Fig. 8. Time history of radial stress and hoop stress for middle point on thickness of each layer

From these figures, the following properties of time history of radial stress and hoop stress were observed:

First, by varying the point of stress from the inner to the outer area of the layered cylinder, both time history variation stresses decreased. Second, the hoop stress is the most sensitive to the V_{CN}^{*} variation. Third, the minimum radial stress occurs when $r = r_{\max} = 50cm$. The effect on the hoop stress plotted in Figures (8c) and (8d) is more involved, with increasing radius. Fourth, the radial distance r has a vital effect on the amplitude of stresses. When r changes from 0.25 to 0.5, amplitude of radial stress and hoop stress decreases. Fifth, time history of hoop stress is more sensitive to variation of r with respect to the time history of radial stress.

CONCLUSIONS

In this article, a multilayer functionally graded nanocomposite cylinder reinforced by carbon nanotubes under shock loadings was analyzed, using the MLPG method. To study the dynamic behaviors of stress filled, meshless local integral equations (LIEs), the MLPG method was applied in displacement domain and Laplace-transform method was employed in the time domain. To simulate the variation of mechanical properties, a micro-mechanical model was used for the problem. The effects of the kind of distribution and volume fraction of CNTs, on the stress wave propagation of CLSRCN are presented in this study. The main results obtained can be expressed as follows:

- The time histories of stresses were studied in detail for some points, on thickness of CLSRCN cylinder and various volume fraction values.
- By increasing the value of V_{CN}^{*}, the values of hoop stresses decreased.
- There is no significant effect of variation in the value of V_{CN}^{*} on amplitude of radial stresses.
- The Λ and X types of grading patterns are more effective on dynamic behaviors of hoop stresses compared to other grading pattern types.
- It is possible to track the wave fronts in stress field for various types of CNTs distributions, using the presented meshless method.
- The presented method can be developed for 2D and 3D elastic wave propagation in CLSRCN with various transient boundary conditions.

REFERENCES

Abate, J. and Valko, P. (2004). “Multi-precision Laplace inversion”, *International Journal for Numerical Methods in Engineering*, 60(5), 979-993.

Bahmyari, E. and Rahbar-Ranji, A. (2012). “Free vibration analysis of orthotropic plates with variable thickness resting on non-uniform elastic foundation by element free Galerkin method”, *Journal of Mechanical Science and Technology*, 26 (9), 2685-2694.

Chen, W.Q., Wang, H.M. and Bao, R.H. (2007). “On calculating dispersion curves of waves in a functionally graded elastic plate”, *Composite Structures*, 81(2), 233–242.

Ching, H.K. and Yen, S.C. (2005). “Meshless local Petrov-Galerkin analysis for 2D functionally graded elastic solids under mechanical and thermal loads”, *Composites Part B: Engineering*, 36(3), 223–240.

Davies, B. (2002). *Integral transforms and their applications*, 3rd Edition, Springer, New York.

Esawi, A.M.K. and Farag, M.M. (2007). “Carbon nanotube reinforced composites: potential and current challenges”, *Materials & Design*, 28(9), 2394–2401.

Gilhooley, D.F., Xiao, J.R., Batra, R.C., McCarthy, M.A. and Gillespie, Jr J.W. (2008). “Two-dimensional stress analysis of functionally graded solids using the MLPG method with radial basis functions”, *Computational Materials Science*, 41(4), 467–481.

Hosseini, S.M., Akhlaghi, M. and Shakeri, M. (2007). “Dynamic response and radial wave propagation velocity in thick hollow cylinder made of functionally graded materials”, *Engineering Computations*, 24(3), 288-303.

Hosseini, S.M. and Abolbashari, M.H. (2010). “General analytical solution for elastic radial wave propagation and dynamic analysis of functionally graded thick hollow cylinders subjected to impact loading”, *Acta Mechanica*, 212, (1-2), 1–19.

Hosseini, S.M. and Shahabian, F. (2011a). “Transient analysis of thermo-elastic waves in thick hollow cylinders using a stochastic hybrid numerical method, considering Gaussian mechanical properties”, *Applied Mathematical Modeling*, 35(10), 4697–4714.

Hosseini, S.M. and Shahabian, F. (2011b). “Stochastic assessment of thermo-elastic wave propagation in functionally graded materials (FGMs) with Gaussian uncertainty in constitutive mechanical properties”, *Journal of Thermal Stresses*, 34(10), 1071–1099.

Iijima, S. (1991). “Helical microtubules of graphitic carbon”, *Nature*, 354(6348), 56-58.

Lu, J.P. (1997). “Elastic properties of single and multilayered nanotubes”, *Journal of Physics and Chemistry of Solids*, 58(11), 1649–52.

Moussavinezhad, S., Shahabian, F. and Hosseini, S.M. (2013). “Two dimensional stress wave propagation in finite length FG cylinders with two directional nonlinear grading patterns using MLPG method”, *Journal of Engineering Mechanics*, 140(3), 575-592.

Seidel, G.D. and Lagoudas, D.C. (2006). “Micromechanical analysis of the effective elastic properties of carbon nanotube reinforced composites”, *Mechanics of Materials*, 38(8), 884–907.

Shen, H.S. (2011). "Postbuckling of nanotube–reinforced composite cylindrical shells in thermal environments, Part I: axially-loaded shells", *Composite Structures*, 93(8), 2096–2108.

Shen, H.S. (2009). "Nonlinear bending of functionally graded carbon nanotube reinforced composite plates in thermal environments", *Composite Structures*, 91(1), 9-19.

Singh, S., Singh, J. and Shukla, K. (2013). "Buckling of laminated composite plates subjected to mechanical and thermal loads using meshless collocations", *Journal of Mechanical Science and Technology*, 27 (2), 327-336.

Singh, J., Singh, S. and Shukla, K. (2011). "RBF-based meshless method for free vibration analysis of laminated composite", *World Academy of Science, Engineering and Technology*, 79, 347-352

Sladek, J., Stanak, P., Han, Z.D., Sladek, V. and Atluri, S.N. (2013). "Applications of the MLPG method in engineering and sciences: A review", Computer Modeling in Engineering & Sciences (CMES), 92(5), 423-475.

Xiao, J.R. and McCarthy, M.A. (2003). "A local heaviside weighted meshless method for two-dimensional solids using radial basis functions", *Computational Mechanics*, 31(3-4), 301–315.

Xiao, J.R., Gilhooley, D.F., Batra, R.C., Gillespie, J.W. and McCarthy, M.A. (2008). "Analysis of thick composite laminates using a higher-order shear and normal deformable plate theory (HOSNDPT) and a meshless method", *Composites Part B: Engineering*, 39(2), 414-427.